

EXPERIMENTAL AND NUMERICAL INVESTIGATION OF FAILURE OF QUASI-BRITTLE MATERIALS

J. Gao and M. L. Wang

Department of Civil Engineering, The University of New Mexico,
Albuquerque, U. S. A.

H. L. Schreyer

Department of Mechanical Engineering, The University of New
Mexico, Albuquerque, U. S. A.

Abstract

Failure modes of cement mortar in compact-tension specimens were studied using the scanning electron microscope (SEM). Microcrack propagation was monitored under large magnification. Starting with a pre-existing notch, it was found that cracks propagated in the nonplanar or tortuous manner. A finite element method was developed based on continuum damage mechanics. Concrete is simulated as a two-phase material of coarse aggregate particles in a mortar matrix. Numerical analysis of a specimen under pure tension was conducted to show similar features of crack propagation.

1 Introduction

The load-displacement (nominal stress-strain) curve of quasi-brittle materials such as cement mortar, concrete, and rock under tension displays a gradual descending branch after the peak load. It is also known as strain softening accompanied by non-homogeneous and highly localized deformations of the specimen (van Mier, 1986; Vonk et al., 1991; Read and Hegemier, 1984; Gopalaratnam and Shah, 1985). The

process behind it is not completely known. Micromechanical models are valuable tools for simulating the mechanical behavior of concrete modelled as a two-phase material using finite element analysis. These models allow a more detailed view of actual material behavior (Bazant et al., 1990; Vonk et al., 1991; Wang et al., 1995)

An understanding of the phenomenological behavior concerning the microfracture process is important as a starting point as well as a guide for developing constitutive relations for quasi-brittle materials. A proper understanding of the mechanism of microcracking can only be gained by direct observation of crack propagation at the microstructural level during loading.

In-situ compact-tension tests were conducted in the SEM chamber to provide direct observation of crack propagation at the microstructural level during loading. It was found that the crack propagation was nonplanar and that branching of the crack existed. This work is in agreement with the observation of Tait et al. (1990).

In microstructural terms, concrete, is an extremely complex system of solid phase, pores, and water, with a high degree of heterogeneity. Concrete consists of coarse aggregate particles, distributed in a matrix of cement mortar; and cement mortar is itself a mixture of sand grains and hydration products of cement (cement paste). The cement paste is an intricate network of crystal (calcium hydroxide and calcium sulfaluminate hydrates) and poorly crystalline compounds (calcium silicate hydrates). The interface between coarse aggregates and mortar is characterized by a higher porosity and a different crystalline network (Scrivener, 1989), as is the interface between sand grains and cement paste.

Based on the microstructure of concrete, the numerical model in two dimensions is established for a small specimen composed of a set of coarse aggregates embedded in cement mortar. Cement mortar is considered as the region of elastic damaging material. An initial assumption is that each grain is isotropic elastic. Numerical simulations of the failure of cement mortar are obtained by the finite element method combined with continuum damage mechanics. A robust algorithm provides solutions in the post peak-load regime and show the essential aspects of the failure process.

2 Experimental studies

2.1 Cement mortar

ASTM Portland cement Type I/II was used in this study. The proportions of materials are one part of cement to 2.75 of sand (sieved through #8 sieve) with water/cement ratio 0.23. Superplasticizer was

used to obtain the required consistency of cement mortar. The cement mortar was cast in a special mold, measuring 1.15 in. (2.92 cm) X 1.15 in. (2.92 cm) X 6 in. (15.24 cm). With this mold two brass tubes with 1/8 in. (0.32 cm) diameter were embedded in the mortar specimen. The specimen was stored in a fog room until stripping. After stripping the mortar was stored under lime saturated water until testing.

2.2 Specimen

The specimens were cut from the cast mortar by a diamond saw into 2 mm thick pieces. The dimensions are shown in Fig. 1. The holes of the specimens were provided by the embedded brass tubes, and the notch was sawed by a thin diamond wafering blade. After machining, the specimens were polished with a 220 mesh diamond disc.

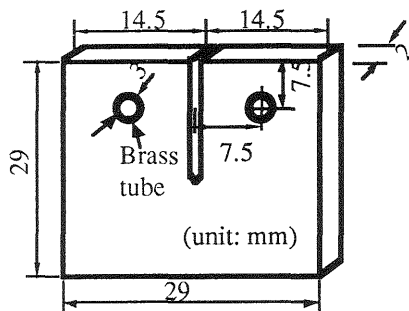


Fig. 1 Geometry of compact-tension specimen

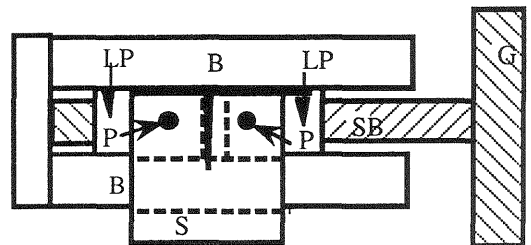


Fig. 2 Schematic of the loading stage: S --- Specimen, P--- Loading Pins, B---Base of loading stage

2.3 Loading stage

Figure 2 shows a tension-compression (T-C) loading device which can be mounted to the SEM position stage. A single sliding brass block (SB) moved in a machined aluminum body assembly (LP). To implement rotation of the lead-screw, a worm and ring gear (40:1 ratio) set-up (G in Fig. 2) was utilized. This set-up greatly reduced reverse rotation and provided a smooth application of lead-screw torque. A square shaft slid in a keyed slot running through the worm gear, and a 90 degree bevel gear system with another square free-sliding shaft was connected through a DelrinTM U-joint to a vacuum rotational-feed-through shaft. This shaft could be rotated by the geared stepper motor for precise feed-back control.

2.4 Experimental results

The load was applied carefully by constantly detecting the notch tip at high magnification. A crack started to propagate from the notch tip after a certain load. The load was maintained, and the entire crack was examined. The profiles of the crack demonstrated crack deflection with the tortuosity of the crack path. The crack propagation of cement mortar which was started from crack tip is shown in Fig. 3, in which the crack propagates from the lower part of the micrograph to the upper part. Crack-deflection processes operate when a crack interacts with microstructurally related features (e.g., weak interfaces between sand and cement paste) that reduce deviation from planarity. As the crack deflects out of the plane normal to the applied stress, the stress intensity at the tip diminishes, reducing the crack driving force and improving the fracture toughness.

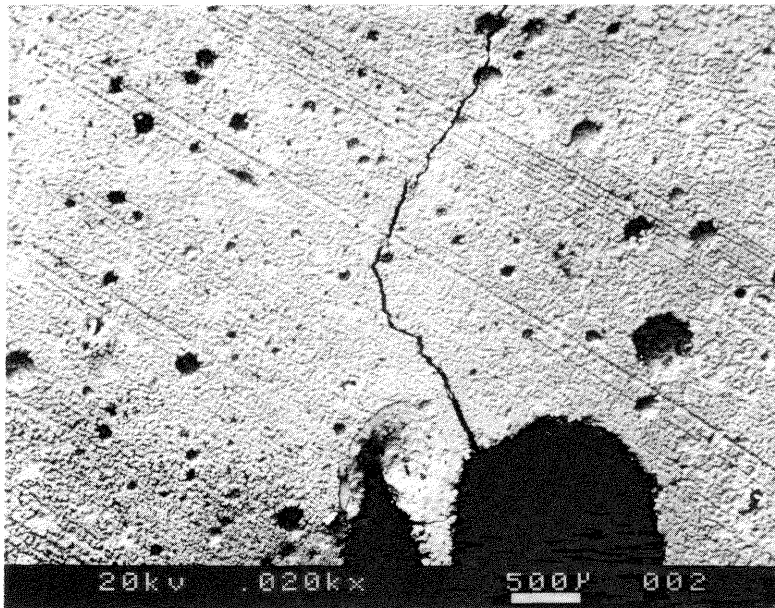


Fig. 3 Crack propagation from the crack tip

Figure 4 shows a crack branching site in the crack wake; it also indicates bridging sites along the profile of the crack. These observations in the compact-tension test confirm some conclusions from the earlier study reported by Tait et al. (1990).

The concrete experiments conducted by Hsu et al. (1963) shows similar results:

1. Cracking in concrete starts at the interface between the coarse aggregates and cement mortar;
2. Continuous crack patterns are created by mortar cracks. Therefore, the mechanical features of the cement mortar must have a significant impact in the mechanical behavior of concrete.

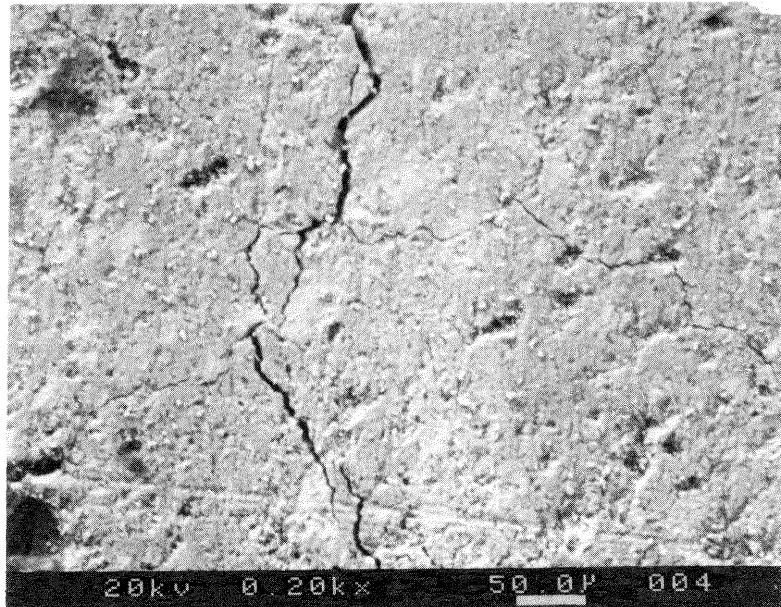


Fig. 4 Crack branch and crack bridging in the wake of crack

3 Analytical formulation

In order to fully understand the fracture process of a quasi-brittle material a constitutive model for the constituents is necessary. In this section, a two-dimensional analysis is proposed in which the coarse aggregate and cement mortar are considered as different materials.

3.1 Finite element meshes

In order to model the internal composite structure of concrete a coarse aggregate is represented as a hexagon, which is discrete with 6 three-node triangular elements. The cement mortar, which is considered uniform and of constant thickness, is located between the coarse aggregates, and represented by small three node triangular elements and four-node quadrilateral elements (Fig. 5a). The type of concrete that was simulated contained aggregates with $3/8$ in. (9.5 mm) diameter and

a coarse aggregate content of 40% (Fig. 5b). The boundary conditions are shown in Fig. 5c.

3.2 Continuum damage mechanics

The nonlinear behavior of quasi-brittle materials is more accurately represented as the evolution of distributed microcracks rather than plastic deformation; therefore, continuum damage mechanics is the most appropriate approach. Some theoretical implications of the use of continuum damage mechanics have been explored as a precursor to the incorporation of essential aspects of microstructural approaches (Ju, 1991; Krajcinovic, et al., 1991) in a sufficiently simple manner to retain the feasibility of performing numerical simulations.

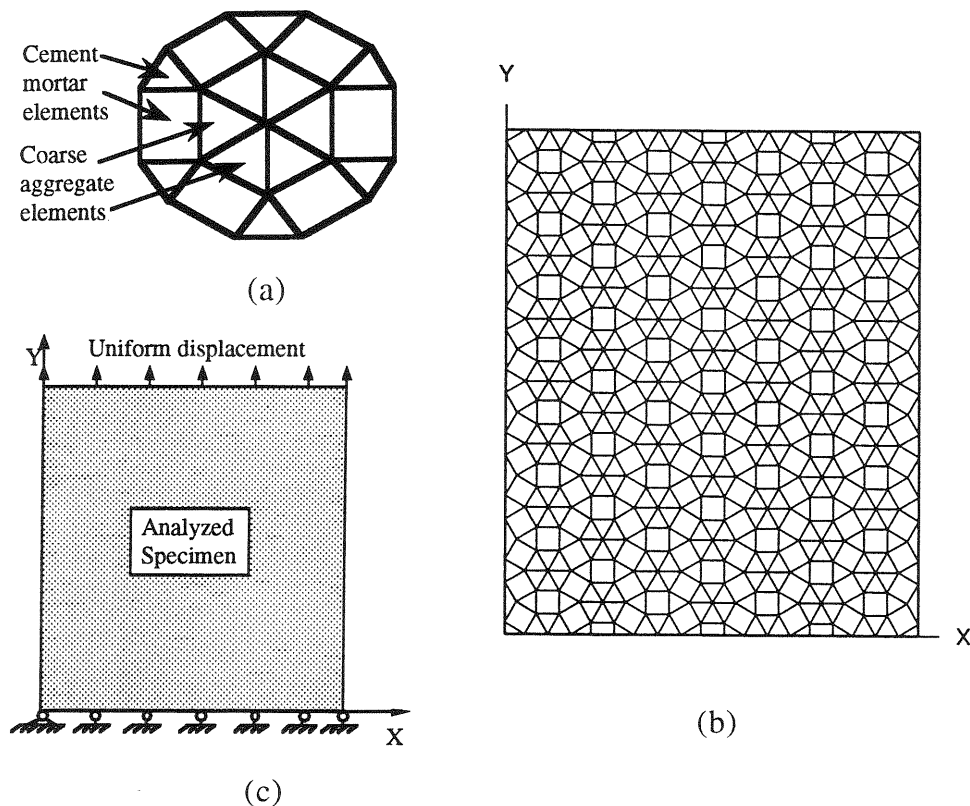


Fig. 5 (a) Coarse aggregate and mortar elements; (a) Finite element mesh for complete specimen; (c) Boundary conditions for the computational specimen

Conventional damage consists of the creation of voids and microcracks which consequently reduce the mechanical properties of a material, such as the bulk and shear moduli. Damage is assumed to be isotropic in this initial approach.

If the thermal effects are ignored, the internal energy, U , is assumed to be a function of the total strain tensor, \mathbf{e} , and the "internal" variable consists of the fourth-order elasticity tensor, \mathbf{E} . With the assumption of linear elasticity, U is taken to be

$$U = \frac{1}{2} \mathbf{e} : \mathbf{E} : \mathbf{e} \quad (1)$$

The application of the first and second (Clausius-Duheim inequality) laws of thermodynamics leads to the constitutive relation for stress, \mathbf{s} ,

$$\mathbf{s} = \frac{\partial U}{\partial \mathbf{e}} = \mathbf{E} : \mathbf{e} \quad (2)$$

and the dissipation inequality

$$-\frac{\partial U}{\partial \mathbf{E}} :: \dot{\mathbf{E}} \geq 0 \quad \text{or} \quad -\frac{1}{2} \mathbf{e} : \dot{\mathbf{E}} : \mathbf{e} \geq 0 \quad (3)$$

Suppose the damage process is parameterized through the use of a parameter, ω , which is monotonically increasing ($\dot{\omega} \geq 0$). The evolution equation for damage can be given as follows:

$$\dot{\mathbf{E}} = -\dot{\omega} \mathbf{R}(\mathbf{E}, \mathbf{e}) \quad (4)$$

in which the dependence of the response function, \mathbf{R} , is shown. Since $\dot{\omega} \geq 0$, the dissipation inequality becomes

$$D = \frac{1}{2} \mathbf{e} : \mathbf{R} : \mathbf{e} \geq 0 \quad (5)$$

which is satisfied if \mathbf{R} is positive definite (conventional definition of damage).

Suppose a damage function, f , is defined such that damage occurs when the state falls on the damage surface, $f = 0$, and for which the dissipation inequality is satisfied automatically. The inequality is met if

$$f = D - g^2(\mathbf{E}, \mathbf{e}) \quad (6)$$

Then when $f < 0$ damage is not occurring, and $f > 0$ is not a physical state. The consistency condition $\dot{f} = 0$ yields an equation for $\dot{\omega}$.

Let \mathbf{I} and \mathbf{i} denote the fourth-order and second-order identity tensors, respectively. The spherical and deviatoric projections are defined as

$$\mathbf{P}^{sp} = \frac{1}{3} \mathbf{i} \otimes \mathbf{i} \quad \mathbf{P}^d = \mathbf{I} - \mathbf{P}^{sp} \quad (7)$$

Then

$$\begin{aligned} \mathbf{P}^{sp} : \mathbf{P}^{sp} &= \mathbf{P}^{sp} & \mathbf{P}^d : \mathbf{P}^d &= \mathbf{P}^d & \mathbf{P}^{sp} : \mathbf{P}^d &= 0 \\ \mathbf{s}^d &= \mathbf{P}^d : \mathbf{s} & \mathbf{e}^d &= \mathbf{P}^d : \mathbf{e} \\ \mathbf{s}^{sp} &= \mathbf{P}^{sp} : \mathbf{s} = -\mathbf{P}\mathbf{i} & \mathbf{e}^{sp} &= \mathbf{P}^{sp} : \mathbf{e} = \frac{1}{3} e_v \mathbf{i} \end{aligned} \quad (8)$$

in which $\mathbf{P} = -(\mathbf{i}:\mathbf{s})/3$ is the mean pressure, $e_v = \mathbf{e}_v : \mathbf{i}$ is the volumetric strain, \mathbf{s}^{sp} and \mathbf{s}^d denote the spherical and deviatoric parts of the stress tensor, respectively, and \mathbf{e}^{sp} and \mathbf{e}^d are the corresponding parts of the strain tensor. With the use of the projection operators, the isotropic elasticity tensor is $\mathbf{E} = 3\mathbf{K}\mathbf{P}^{sp} + 2\mathbf{G}\mathbf{P}^d$ in which \mathbf{K} is the bulk modulus and \mathbf{G} is the shear modulus. Both parameters may change with damage.

For the initial numerical investigation performed for this study, g was chosen to be a constant and \mathbf{R} to be the isotropic elastic tensor \mathbf{E} . The result is a simple scalar isotropic damage model in which the bulk and shear moduli decay simultaneously with ω . A slightly more general model is then introduced in which \mathbf{R} is an isotropic tensor not proportional to \mathbf{E} . The result is a two parameter isotropic damage model in which the bulk and shear moduli deteriorate at different rates. The two damage models are discussed in subsequent sections.

3.3 Plane stress elasticity

The two-dimensional elastic matrix $[\mathbf{E}]$ is introduced such that

$$\{\boldsymbol{\sigma}\} = [\mathbf{E}] \{\mathbf{e}\} \quad (9)$$

in which $\{\boldsymbol{\sigma}\}^T = \langle \sigma_{xx}, \sigma_{yy}, \sqrt{2}\sigma_{xy} \rangle$ and $\{\mathbf{e}\}^T = \langle e_{xx}, e_{yy}, \sqrt{2}e_{xy} \rangle$ are vectors of stress and strain components, respectively. The coefficient $\sqrt{2}$ of the shear component is used so that the two-norm is preserved.

For the plane stress isotropic problem,

$$[E] = \frac{E}{1-\mu^2} \begin{bmatrix} 1 & \mu & 0 \\ \mu & 1 & 0 \\ 0 & 0 & 1-\mu \end{bmatrix} = \begin{bmatrix} \frac{3(1-2\mu)K}{1-\mu^2} & \frac{3\mu(1-2\mu)K}{1-\mu^2} & 0 \\ \frac{3\mu(1-2\mu)K}{1-\mu^2} & \frac{3(1-2\mu)K}{1-\mu^2} & 0 \\ 0 & 0 & 2G \end{bmatrix} \quad (10)$$

in which E and μ are Young's modulus and Poisson's ratio, respectively. The volumetric strain is

$$e_v = e_{xx} + e_{yy} + e_{zz} = \frac{1-2\mu}{1-\mu} (e_{xx} + e_{yy}) \quad (11)$$

3.4 Isotropic damage model

An evolution equation is obtained with the following choice of \mathbf{R} :

$$\mathbf{R} = 3 \alpha K \mathbf{P}^{sp} + 2 \beta G \mathbf{P}^d \quad (12)$$

in which α and β are chosen to be constant. Substitute Eq. (12) into Eq. (4) to obtain

$$\dot{K} = -\alpha \dot{\omega} K \quad \dot{G} = -\beta \dot{\omega} G \quad (13)$$

or

$$K = K_0 e^{-\alpha\omega} \quad G = G_0 e^{-\beta\omega} \quad 0 \leq \omega \leq \infty \quad (14)$$

in which K_0 and G_0 are the initial values of the bulk and shear moduli, respectively.

The substitution of Eqs. (5) and (12) into Eq. (6) yields the damage function

$$f = \frac{1}{2} (\alpha K e_v^2 + 2\beta G \mathbf{e}^d : \mathbf{e}^d) - g^2 \quad (15)$$

Suppose $g = g_0$ is a constant chosen so that under uniaxial tensile stress, damage initiates at a tensile stress of σ_0 in the x -direction. The corresponding non-zero components of strain are

$$e_{xx} = \frac{\sigma_0}{E_0}, \quad e_{yy} = e_{zz} = -\mu_0 \frac{\sigma_0}{E_0} \quad (16)$$

in which E_0 and μ_0 are the initial values of Young's modulus and Poisson's ratio respectively. Then

$$g^2 = \left(\frac{\sigma_0}{E_0}\right)^2 \left[\frac{K_0}{2} (1-2\mu_0)^2 + \frac{G_0}{3} (2+4\mu_0+2\mu_0^2) \right] \quad (17)$$

The consistency condition together with the use of Eq. (13) yields

$$\dot{\omega} = \frac{2(\alpha K e_v \dot{e}_v + 2 \beta G e^d : \dot{e}^d)}{\alpha^2 K e_v^2 + 2 \beta^2 G e^d : e^d} \quad (18)$$

It is assumed that the damaging regions are confined to the cement mortar, so the evolution equation of the elastic parameters for the cement mortar assume the form given by Eq. (14). With this damage model, if $\alpha = \beta = 1$, Young's modulus E becomes

$$E = \frac{9KG}{3K+G} = e^{-\omega} E \quad (19)$$

and the bulk modulus, the shear modulus and Young's modulus decrease at the same rate. However, Poisson's ratio μ remains constant:

$$\mu = \frac{3K - 2G}{2(3K + G)} = \mu_0 \quad (20)$$

With $\alpha=1$, if $\beta > 1$ then G decays faster than K ; if $\beta < 1$ then G decays slower than K , or vice versa. For those cases, E follows a more complicated evolution equation and Poisson's ratio is not a constant, which is a more realistic feature of experimental data. For quasi-brittle materials, the volumetric strain rate can actually approach zero under uniaxial compression which implies a Poisson's ratio of $\frac{1}{2}$; therefore $\beta > 1$ is representative of features exhibited by compressive loading. Here, the loading is tensile so the opposite case of $\beta < 1$ is considered.

It should be emphasized that damage is generally an anisotropic process so the assumption of isotropy is a severe simplification introduced to make the analysis tractable. The parameters α and β merely provide a technique for evaluating the relative effect of loss of stiffness for the bulk and shear moduli.

3.5 Dynamic relaxation and CoMeT

In finite element codes, dynamic relaxation (DR) is often used as an explicit incremental method for solving static problems. Use of the dynamic relaxation method simplifies the software. Since the method is explicit, it is unnecessary to form a global stiffness matrix; therefore, much less computer storage is needed than with implicit procedures such as Newton-type method (Underwood, 1983).

The whole modeling process was accomplished by coupling the nonlinear dynamic relaxation analysis program with the program CoMeT (Computational Mechanics Toolkit) and an interactive graphical shell for integrated computational mechanics. For each iteration, the new damage values of K and G were calculated in terms of a current damage parameter at each Gaussian point. After one step was finished, a data-base file was output that could be processed by CoMeT.

3.6 Numerical results

To illustrate the proposed damage model, sample problems were considered. The coarse aggregate themselves were assumed to be isotropic, linearly elastic with typical values for coarse aggregate chosen to be $E^A=10.2E6$ psi (70 GPa), and $\mu^A = 0.22$, with a corresponding bulk modulus $K^A= 6.2E6$ psi (42.9 GPa) and shear modulus $G^A = 4.15E6$ psi (28.6 GPa). It is assumed that a stress state high enough to cause damage in the coarse aggregates does not occur. The damage formulation is, therefore, applied only to the material in the cement mortar for which the initial properties are assumed to be $E_0= 3.6E6$ psi (25 GPa) and $\mu_0= 0.25$ which correspond to $K_0 = 2.4E6$ psi (16.7 GPa) and $G_0 = 1.5E6$ psi (10 GPa). The peak value of uniaxial stress in tension is taken to be 800 psi (5.5 MPa) which yields a value of $g^2 = 0.5$ from Eq. (17).

To illustrate the basic feature of the model for concrete in tension, an analysis was first performed for $\alpha=\beta=1.0$. In this case, the shear modulus decreases at the same rate as the bulk modulus.

The macroscopic nominal stress-strain curve for the concrete is shown in Fig. 6. The nominal strain is defined as the prescribed displacement on the top boundary divided by the original length of the specimen. In the same manner, the nominal stress is defined as the corresponding sum of nodal forces at the top surface divided by the original cross-section area. Also shown in Fig. 6 is the stress-strain behavior based on the proposed damage model under uniaxial tensile loading of the cement mortar material. Structural softening is much more abrupt than that shown for the mortar because, when failure occurs, a significant part of the specimen unloads elastically.

The stress-strain curve shows that the concrete has the tensile stress of 700 psi (4.8 MPa), and the corresponding peak strain is 180×10^{-6} , which are typical values for concrete under tension.

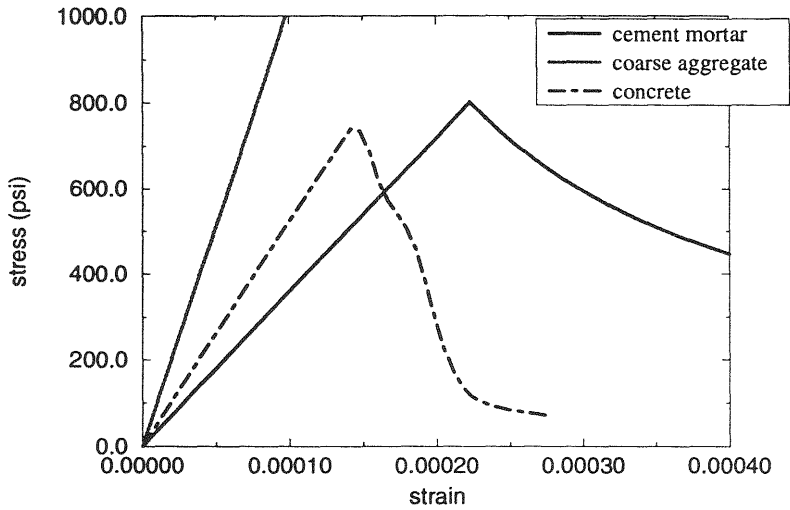


Fig. 6 Macroscopic nominal stress-strain behavior

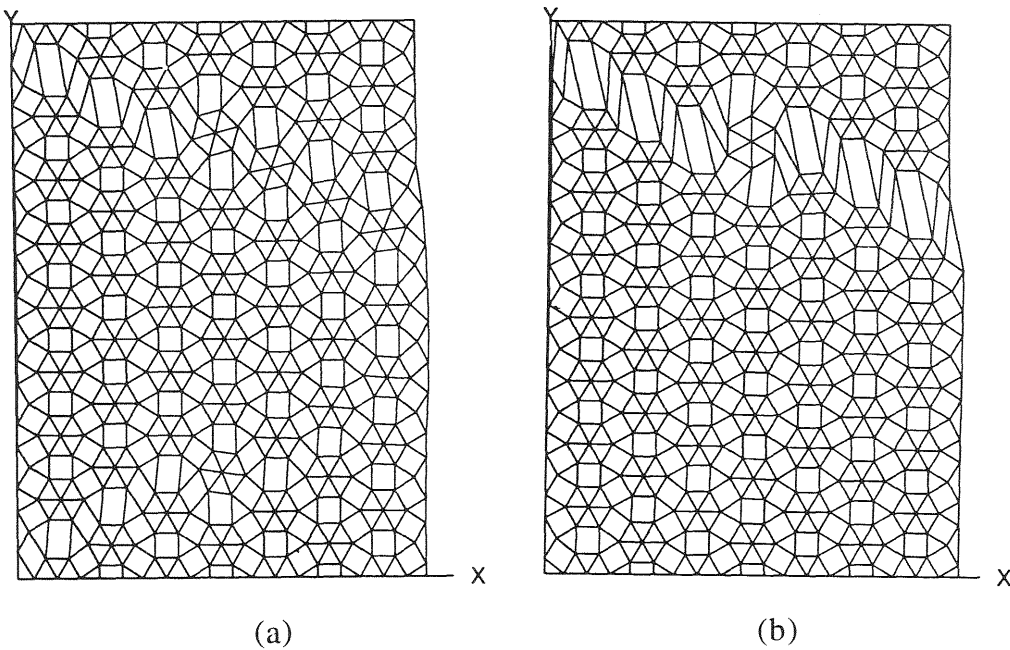


Fig. 7 (a) Deformed mesh at 77% of the prescribed maximum strain; (b) deformed mesh at 100% of the prescribed maximum strain

The deformed meshes at the prescribed nominal strains of 77% and 100% of the maximum nominal strain [275×10^{-6}] are shown in Fig. 7a and 7b. Fig.7a shows that several microcracks initiate and start to propagate. This situation can be interpreted as the creation of microcracks under tension, which has been shown by other researchers (Hoagland, et al, 1980). When the loading increases, a main crack propagates, and crack branching and bridging occur as shown in Fig. 7b. Significant rotations of coarse aggregate rotation can be observed in the deformed mesh.

4 Conclusions

To provide some insight into the micromechanical features of crack propagation of concrete, the specimen under tension was investigated numerically. The results of the simulations show that the model is able to describe qualitatively the softening of concrete. The overall stress strain curve shows the typical values of concrete mechanical properties.

To account for the possible slower deterioration of the shear modulus which might occur with, for example, the presence of fibers, the possible computations should be performed using higher values of β .

The first results of the micromechanical research presented here have been encouraging and further analysis of the compressive softening mechanism will be carried out. Another extension of this research will be the study of fiber-reinforce concrete

5 References

- Bazant, Z. P., Tabbara, M. R., Kazemi, M. T. and Pijaudier-Cabot, G. (1990) Random particle model for fracture of aggregate of fiber composites. **J. Engrg. Mech.**, 106, 1686-1705.
- Gopalaratnam, V. S. and Shah, S. P. (1985) Softening response of plain concrete in direct tension. **J. Am. Concr. Inst.**, 82, 310-323.
- Hoagland, R. G. and Embury, J. D. (1980) A treatment of inelastic deformation around a crack tip due to microcracking. **J. Am. Ceram. Soc.**, 63, 404-410.
- Hsu, T. T. C., Slate, F., Sturman, G. and Winter, G. (1963) Microcracking of plain concrete and the shape of the stress-strain curve. **J. Am. Concr. Inst.**, 60, 209-224.

- Ju, J. W. (1991) On two-dimensional self-consistent micromechanical damage models for brittle solids. **Int. J. Solid & Struct.**, 27, 227-258.
- Krajcinovic, D., Basista, M. and Sumarac, D. (1991) Micromechanically inspired phenomenological damage model. **J. Appl. Mech.**, 58, 305-310.
- Read, H. E. and Hegemier, G. A. (1984) Strain-softening of rock, soil, and concrete--A review article. **Mech. Mater.**, 3, 271-294.
- Scrivener, K. L. (1989) The microstructure of concrete, in **Materials Science of Concrete I** (ed. by J. P. Skalny), The American Ceramic Society Inc., Ohio, U. S. A., 127-162.
- Tait, R. B., Diamond, S., Akers, S. A. S. and Mindess, S. (1990) Microprocess failure zone studies using an in-situ scanning electronic microscope double torsion test facility, in **Proceedings of the symposium on Micromechanics of Failure of Quasi-Brittle Materials** (eds. S. P. Shah, S. E. Swartz and M. L. Wang), Elsevier Applied Science, London, 52-61.
- Underwood, P. (1983) Dynamic relaxation, in **Computational Methods in Mechanics for Transient Analysis** (eds. T. Belytschko and T. J. R. Hughes), North-Holland Publishing, Amsterdam, The Netherlands, 245-65.
- van Mier, J. G. M. (1986) Fracture of concrete under complex stress. **HERON** 36 (3).
- Vonk, R. A., Rutten, H. S., van Mier, J. G. M. and Fijneman, H. L. (1991) Micromechanical simulation of concrete softening, in **Fracture Processes in Concrete, Rock, and Ceramics** (eds. J. G. van Mier, J. G. Rots and A. Bakker), E.&F.N. Spon, London, 129-138.
- Wang, M. L., Gao, J. and Schreyer, H. L. (1995) Experimental and numerical investigation of failure of alumina under plane stress. **J. Engrg. Mech.**, to be published.
- Yazdani, S. and Schreyer, H. L. (1988) An anisotropic damage model with dilatation for concrete. **Mech. Mater.**, 7, 231-244.